# TIME-DEPENDENT HOMOGENIZATION FOR PRESSURIZED HEAVY-WATER REACTORS

**Peter Schwanke and Eleodor Nichita**

Faculty of Energy Systems and Nuclear Science, Ontario Tech University
2000 Simcoe Street North, Oshawa, Ontario, Canada L1G 0C5

peter.schwanke@ontariotechu.ca, eleodor.nichita@ontariotechu.ca

## ABSTRACT

A new time-dependent homogenization approach that accounts for inter-assembly leakage has recently been proposed. The new technique extends Generalized Equivalence Theory (GET) to transient simulations through the use of time-dependent, leakage-corrected discontinuity factors that are calculated at each time step by means of a global-local iterative approach to account for the effect of neighbouring nodes so that highly heterogeneous cores are more accurately modelled than when employing single-node, zero-node-boundary-current Assembly Discontinuity Factors (ADFs). The technique has been previously tested for a one-dimensional, two-energy-group, BWR-like benchmark. The present work expands the analysis to a one-dimensional, two-energy-group, Pressurized Heavy-Water Reactor (PHWR) configuration. The PHWR configuration consists of 22 fuel nodes bounded on either side by two nodes of heavy-water ($D_2O$) reflector. Each fuel node spans 28.575 cm and is a one-dimensional stylized representation of a 37-element, natural uranium fuel bundle with $D_2O$ coolant residing in a pressure tube that in turn resides in a calandria tube surrounded by $D_2O$ moderator. A simple transient induced by instantaneous half-core voiding of the $D_2O$ coolant is studied. Three types of calculations are performed: A reference, heterogeneous-node, fine-mesh calculation, a standardly-homogenized-node calculation and a GET-homogenized-node (using ADFs) calculation. The root-mean-square percent errors introduced by standard homogenization and ADF-based homogenization for kinetics calculations in PHWR cores are found to be 4% and 5%, respectively, after 0.5 s. This suggests that the use of a time-dependent homogenization method is desirable, and its use is shown to reduce the RMS errors to a maximum of 0.003% over the course of the transient. The conclusion is that although PHWR cores are not extremely heterogeneous, the accuracy of transient modelling for PHWRs is improved when using time-dependent homogenization over conventional ADFs and that the newly-developed time-dependent homogenization method promises to offer substantial improvements in accuracy for transient results with particular relevance to safety analyses.

KEYWORDS: time-dependent homogenization, time-dependent discontinuity factors, PHWR

## 1. INTRODUCTION

A new technique was recently presented [1] that extends Generalized Equivalency Theory (GET) [2] to time-dependent problems by determining homogenized nuclear parameters and discontinuity factors at each time step using a global-local iterative scheme. The technique was applied to a one-dimensional (1D), two-energy-group (2G), seven-assembly, boiling-water reactor (BWR) benchmark in which a step-reduction in

the absorption cross sections was introduced in two of the assemblies. The results of the transient simulation using the developed technique showed excellent agreement (to within 0.025%) of the reference solution. In the current work, the technique is applied to a 1D, 2G pressurized heavy-water reactor (PHWR) model. A distinguishing characteristic of the PHWR model is that each fuel node consists of a central fuel region of natural uranium surrounded by a significant amount heavy-water ($D_2O$) moderator whereas for the BWR model, the fuel region consists of enriched uranium that occupies the majority of the node such that the moderator region, comprised of light water, is much smaller. Consequently, the fuel nodes of the PHWR model exhibit a higher degree of heterogeneity across the node than those of the BWR model. Furthermore, the BWR model is a seven-assembly configuration that uses reflective boundaries at the either end of the reactor model whereas the PHWR model is a 22-fuel-node configuration that has two additional reflector nodes of $D_2O$ at either end of the reactor model where vacuum boundaries are applied. The presence of the reflector nodes introduces a homogenization challenge that is addressed in the present work. A transient is introduced in the PHWR model by voiding 11 of the 22 fuel nodes in one half of the core resulting in a power rise that is followed for 0.5 s using a time-step of 0.0005 s. The node-averaged results of the transient from a full-core heterogeneous (reference) solution are compared to the homogeneous-node results of the global-local iterative scheme as well as to those of a standardly-homogenized-node calculation and a GET-homogenized-node calculation using assembly discontinuity factors.

## 2. DESCRIPTION OF THE PHWR MODEL

The fuel node of the PHWR model is comprised of a 37-element, natural uranium fuel bundle with $D_2O$ coolant residing in a pressure tube that in turn resides within a calandria tube surrounded by $D_2O$ moderator, as shown in the *Detailed Geometry* of Fig 1. The pressure and calandria tubes are separated by an annular gap that is filled with $CO_2$ gas.

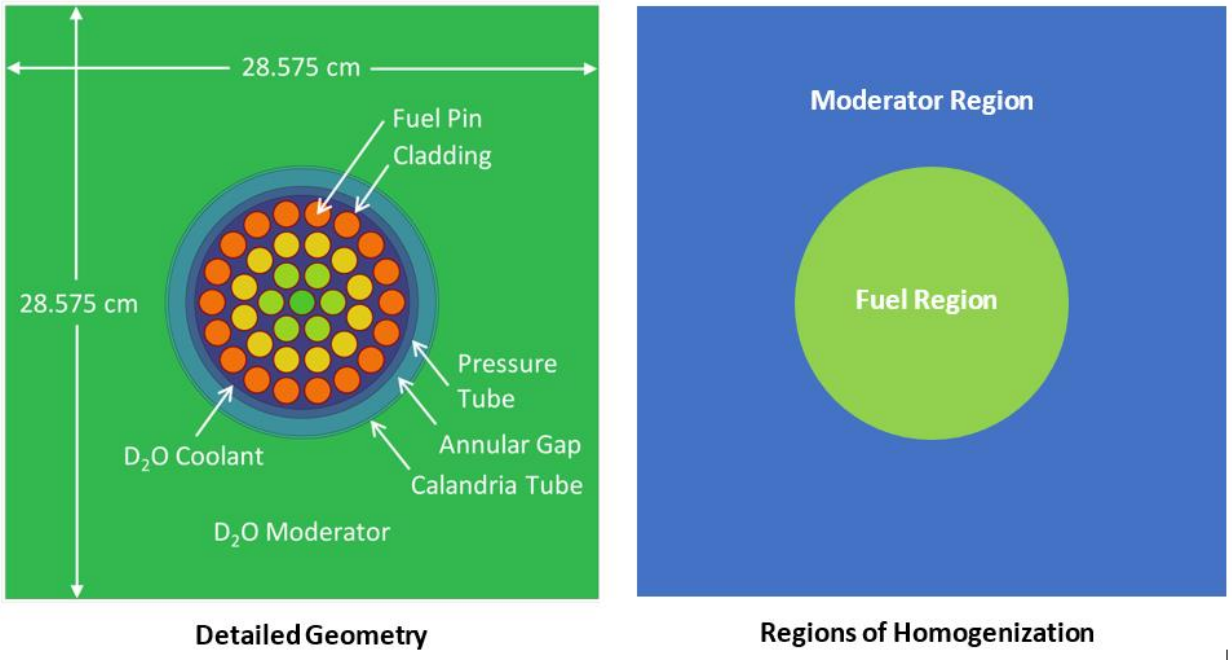


**Figure 1. PHWR Fuel Node**

The transport code DRAGON 3.06 [3] is used to conduct a two-dimensional lattice calculation of the detailed-geometry fuel node using the JEFF 69-energy-group nuclear data library [4]. The lattice calculation is conducted for zero burnup (i.e. fresh fuel) and uses zero-net-current boundary conditions. The resulting macroscopic cross sections are collapsed to two energy groups and homogenized over the fuel and moderator regions shown in Fig. 1 in the *Regions of Homogenization* where the fuel region includes the fuel pins and coolant as well as the calandria tube, the annular gap, and the pressure tube. For the reflector, the cross sections from the detailed-geometry fuel node are homogenized over a 0.1 cm wide strip of moderator at the periphery of the fuel node. The fuel, moderator and reflector cross sections are applied to the 1D, 2G full-core PHWR model, which is depicted in Fig. 2 for the left half of the core showing two reflector nodes and eleven fuel nodes with black lines demarcating the node boundaries.

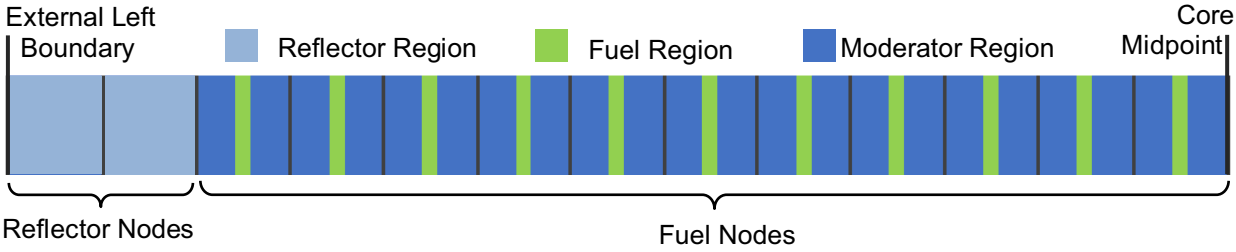


**Figure 2. One-dimensional Heterogenous-Node PHWR Model (Half-core Representation)**

Each node in Fig. 2 spans 28.575 cm and within the fuel nodes the width of the fuel region is such that the ratio of the length of the fuel region to that of the entire fuel node in the 1D model is equal to the ratio of the area of the fuel region to the area of the entire 2D fuel node shown in Fig. 1. The nuclear parameters obtained from DRAGON and used in the 1D, 2G PHWR model are presented in Table I in which $\Sigma_a^1$ and $\Sigma_a^2$ represent the group 1 and 2 macroscopic neutron absorption cross sections, $\nu\Sigma_f^1$ and $\nu\Sigma_f^2$ represent the group 1 and 2 macroscopic neutron production cross sections, $\Sigma_s^{1\to2}$ represents the macroscopic cross section for down-scattering from group 1 to 2, $\Sigma_s^{2\to1}$ represents the macroscopic cross section for up-scattering from group 2 to 1, and $D^1$ and $D^2$ represent the group 1 and 2 diffusion coefficients.

**Table I. Nuclear Parameters of the Heterogeneous PHWR Model under Cooled Conditions**

| Parameter | Fuel Region | Moderator Region | Reflector Region |
|---|---|---|---|
| $\Sigma_a^1$ ($cm^{-1}$) | $6.754\times10^{-3}$ | $3.871\times10^{-6}$ | $3.620\times10^{-6}$ |
| $\Sigma_a^2$ ($cm^{-1}$) | $3.081\times10^{-2}$ | $4.483\times10^{-5}$ | $4.518\times10^{-5}$ |
| $\Sigma_s^{1\to2}$ ($cm^{-1}$) | $1.506\times10^{-3}$ | $1.116\times10^{-2}$ | $1.269\times10^{-2}$ |
| $\Sigma_s^{2\to1}$ ($cm^{-1}$) | $2.048\times10^{-4}$ | $5.125\times10^{-5}$ | $4.920\times10^{-5}$ |
| $\nu\Sigma_f^1$ ($cm^{-1}$) | $3.452\times10^{-3}$ | 0 | 0 |
| $\nu\Sigma_f^2$ ($cm^{-1}$) | $3.864\times10^{-2}$ | 0 | 0 |
| $D^1$ (cm) | 1.409 | 1.271 | 1.268 |
| $D^2$ (cm) | 1.238 | 0.844 | 0.842 |
| **Region Width (cm)** | 4.771 | 11.902 | 28.575 |

## 3. REFERENCE SOLUTION

### 3.1. Steady-state Reference Values

Applying the parameters in Table I to the full-core PHWR model yields the neutron flux distribution shown in Fig. 3. The flux is determined by solving the 1D, 2G, neutron diffusion equation using a mesh-centered, finite-difference discretization in which each material region within a node defines a mesh. For the reflector region, each reflector node is divided into three equally spaced meshes of 9.525 cm with vacuum boundary conditions applied to the external boundaries of the reactor. The resulting flux solution in Fig. 3 constitutes the heterogeneous solution for the 1D, 2G full-core, steady state configuration.

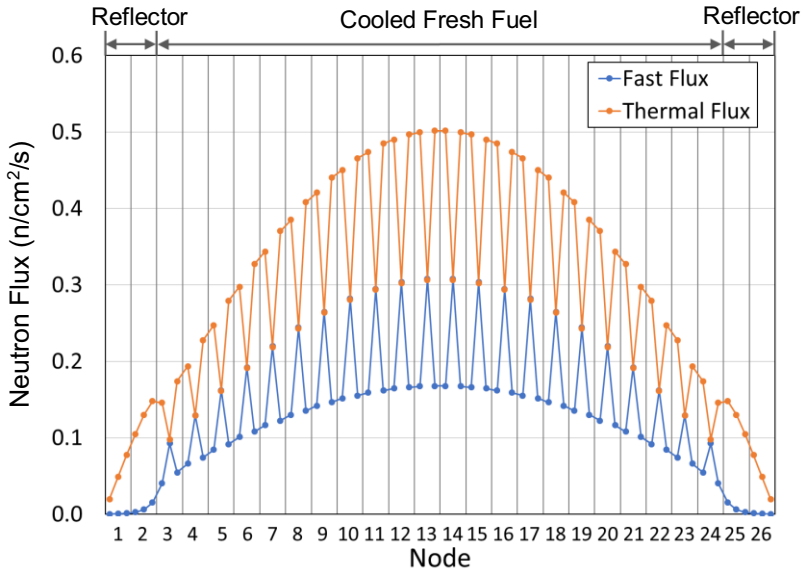


**Figure 3. Heterogeneous, Steady-state Neutron Flux Distributions**

The fluxes in Fig. 3 are normalized to a total fission-neutron production rate of 1 neutron/s. Fig. 3 shows a high degree of heterogeneity across each fuel node with the fast flux being over 1.5 times higher in the fuel region than in the moderator region while the thermal flux is over 1.5 times higher in the moderator region than in the fuel region. In the fuel region, the fast and thermal fluxes are nearly equal. Calculating the node-averaged fluxes from the heterogenous reference solution yields the neutron flux distributions shown in Fig. 4, which also includes the node-integrated fission-neutron production rates. The values in Fig. 4 serve as the reference values for the steady-state configuration against which the results of the global-local iterative process and the traditional homogenization techniques are compared.

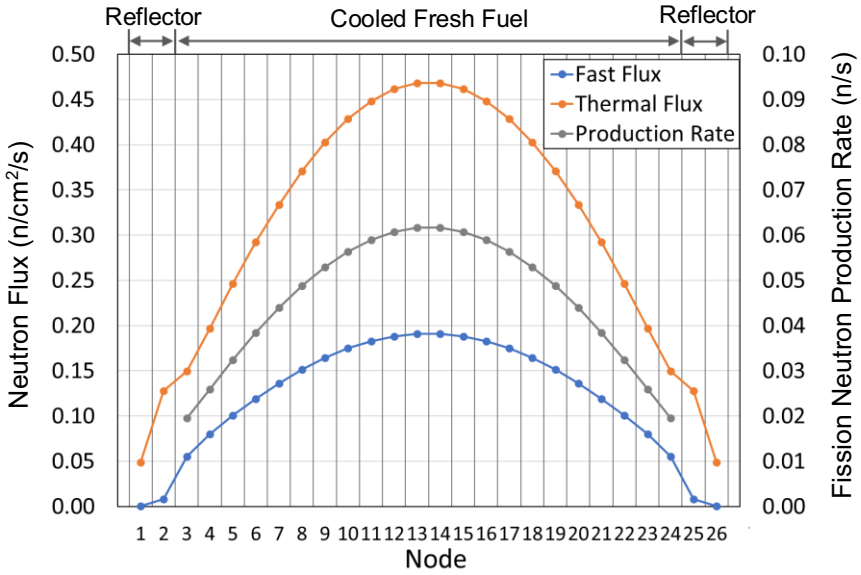


**Figure 4. Reference Node-averaged Neutron Fluxes and Node-integrated Fission-Neutron Production Rates for the Steady-state Configuration**

### 3.2. Transient Reference Values

A transient is initiated in the 1D, 2G PHWR model by voiding the $D_2O$ coolant in the fuel region of the fuel nodes to the left of the core midpoint. A lattice calculation similar to that conducted for the fuel node under cooled conditions is conducted for the fuel node under voided conditions using DRAGON [3]. Only the nuclear parameters for the fuel region are used in the voided fuel nodes of the PHWR model. The nuclear parameters for the moderator regions of the voided fuel nodes are kept the same as those used for the cooled fuel nodes. The nuclear parameters for the fuel region of the voided fuel node are presented in Table II.

**Table II. Nuclear Parameters for the PHWR Fuel Node under Voided Conditions**

| Parameter | Fuel Region | Parameter | Fuel Region |
|---|---|---|---|
| $\Sigma_a^1$ ($cm^{-1}$) | $6.398\times10^{-3}$ | $\Sigma_a^2$ ($cm^{-1}$) | $3.218\times10^{-2}$ |
| $\Sigma_s^{1\to2}$ ($cm^{-1}$) | $4.313\times10^{-4}$ | $\Sigma_s^{2\to1}$($cm^{-1}$) | $1.870\times10^{-4}$ |
| $\nu\Sigma_f^1$ ($cm^{-1}$) | $3.642\times10^{-3}$ | $\nu\Sigma_f^2$ ($cm^{-1}$) | $4.054\times10^{-2}$ |
| $D^1$ (cm) | 1.874 | $D^2$ (cm) | 1.637 |

The voided fuel parameters are introduced at time 0 to initiate a step-change transient. The transient is modelled in increments of 0.0005 s for a total transient duration of 0.5 s. The kinetics parameters used for the transient are presented in Table III. Because zero-burnup (i.e. fresh) fuel is used in the model, the sole contributor of the delayed neutrons is assumed to arise from the fission of U-235. The delayed neutron fractions are thus determined as the ratios of the delayed neutron yields, provided by [5] for U-235, to the total neutron yield, provided by [6]. The decay constants for the precursors are also provided by [5] while the neutron velocities are obtained from [7].

**Table III. Kinetics Parameters (Refs. [5-7])**

| Parameter | Delayed Neutron Group | | | | | |
|---|---|---|---|---|---|---|
| | 1 | 2 | 3 | 4 | 5 | 6 |
| Decay Constant ($s^{-1}$) | 0.0129 | 0.0311 | 0.1340 | 0.3310 | 1.2600 | 3.2100 |
| Delayed Neutron Yield for U-235 | 0.060 | 0.364 | 0.349 | 0.628 | 0.179 | 0.070 |
| Total Neutron Yield for U-235 | 2.418 | | | | | |
| Average Neutron Velocities (cm/s) | $1 \times 10^7$ [group 1 (fast)] | | | $3 \times 10^5$ [group 2 (thermal)] | | |

Fig. 5 shows the resultant node-averaged neutron flux distribution at 0.5 s into the transient along with the node-integrated fission-neutron production rates. At 0.5 s the total fission-neutron production rate for the core has risen to 39.6 n/s.

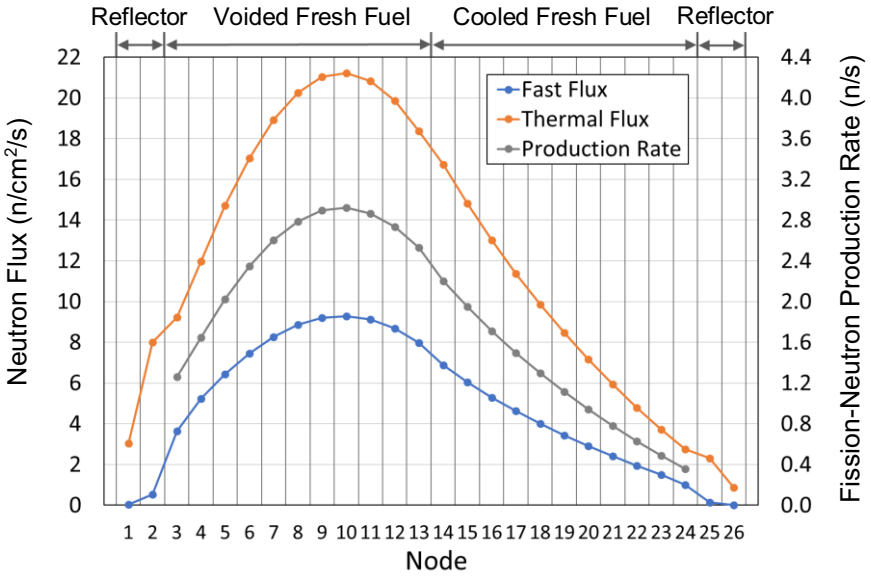


**Figure 5. Reference Node-averaged Neutron Fluxes and Node-integrated Fission-Neutron Production Rates at Transient Time 0.5 s**

## 4. HOMOGENIZATION TECHNIQUES

### 4.1. Standard Homogenization

The standard approach for homogenization is to conduct a single assembly (i.e. single-node) calculation from which the heterogeneous flux is used to homogenize the nuclear parameters over the node. Such

calculations, referred to as assembly calculations, use zero net-currents at the node boundaries and as such do not account for any variations in the average flux of the neighbouring nodes that would be present in an actual core configuration. Assembly calculations are typically done using transport codes such as DRAGON but in the current investigation the heterogeneous flux is determined by solving the neutron diffusion equation for the 1D, 3-region (i.e. moderator-fuel-moderator) fuel node under cooled and voided conditions. The resulting flux is used to homogenize the nuclear parameters over of the given node, the values for which are presented in Table IV.

**Table IV. Node-homogenized Parameters for the Cooled and Voided Fuel Nodes**

| Parameter | Cooled Fuel Node | Voided Fuel Node |
|---|---|---|
| $\Sigma_a^1$ (cm$^{-1}$) | $1.819\times10^{-3}$ | $1.686\times10^{-3}$ |
| $\Sigma_a^2$ (cm$^{-1}$) | $3.411\times10^{-3}$ | $3.530\times10^{-3}$ |
| $\Sigma_s^{1\to2}$ (cm$^{-1}$) | $8.563\times10^{-3}$ | $8.337\times10^{-3}$ |
| $\Sigma_s^{2\to1}$ (cm$^{-1}$) | $6.804\times10^{-5}$ | $6.597\times10^{-5}$ |
| $\nu\Sigma_f^1$ (cm$^{-1}$) | $9.282\times10^{-4}$ | $9.581\times10^{-4}$ |
| $\nu\Sigma_f^2$ (cm$^{-1}$) | $4.227\times10^{-3}$ | $4.397\times10^{-3}$ |
| $D^1$ (cm) | 1.308 | 1.430 |
| $D^2$ (cm) | 0.887 | 0.930 |
| **Node Width (cm)** | 28.575 | 28.575 |

Fig. 6 shows the 1D homogeneous-node PHWR model to which the parameters in Table IV are applied for the steady-state and the transient cases. In both cases the parameters for the reflector nodes are the same as those used in the heterogeneous-node model presented in Table I.

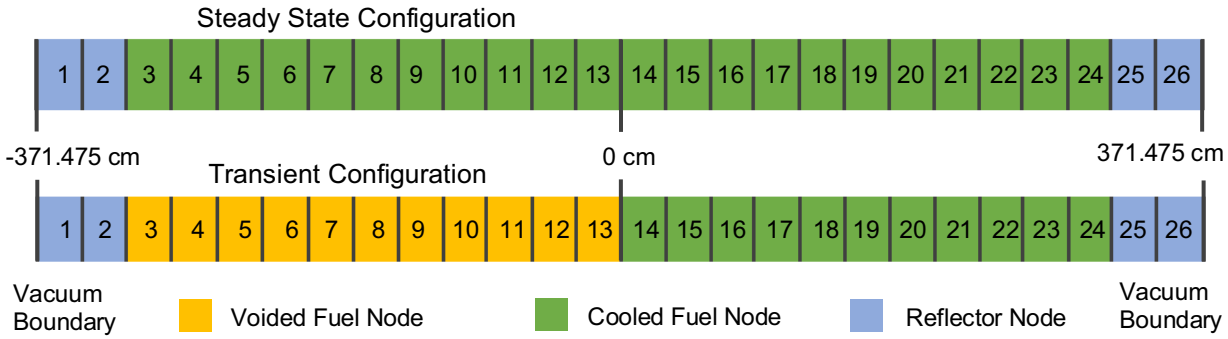


**Figure 6. One-dimensional Homogeneous-Node PHWR Model**

For the standard homogenization solution, the parameters used for the transient configuration remain fixed during the transient and discontinuity factors are not used to maintain equivalency of the node fluxes and reaction rates between the homogeneous-node and the heterogeneous-node solutions.

### 4.2. Homogenization with Assembly Discontinuity Factors

A refinement of the standard homogenization technique discussed in the previous section is to use discontinuity factors (DFs), which are defined as the ratio of the flux at the surface of the heterogeneous node to the flux at the surface of the homogeneous node. From the single assembly calculations previously described, assembly discontinuity factors (ADFs) can be obtained for the cooled and voided fuel nodes. Because zero-net-current boundary conditions are employed the heterogenous flux at the node boundaries will be identical which means there is no variation in the ADFs between the left and right node boundaries. Hence, ADFs do not account for the inter-assembly leakage between neighbouring nodes that would be present in an actual core configuration. The group-dependent ADFs used in the 1D, 2G PHWR model of Fig. 6 are presented in Table V. Note that for the reflector nodes, the ADFs are simply taken to be unity.

**Table V. Assembly Discontinuity Factors**

| Cooled Fuel Node | Voided Fuel Node | Reflector Node |
|---|---|---|
| 0.878 | 0.885 | 1.000 |
| 1.069 | 1.070 | 1.000 |

### 4.3. Time-dependent Homogenization

The time-dependent homogenization technique in [1] updates the nuclear parameters for every node in the PHWR model in response to the changes in the local flux occurring within each node at each time step. The DFs are also updated for every node at every time step by accounting for the changes in the boundary conditions that occur for each node due to the global variation in the flux across the core. In this manner, the DFs are leakage-corrected at each time step. A single-heterogeneous-node calculation (i.e. local calculation) is conducted for each fuel node using the node-specific flux-to-current boundary conditions obtained from the full-core solution (i.e. global calculation). The updated nuclear parameters and DFs are then used in a subsequent global calculation to update the boundary conditions for each node. The global-local calculations are repeated at each time step until convergence is achieved. For the reflector nodes, the absence of fuel means that a single-node calculation is not possible. Instead, a 3-node extended assembly calculation [8] is conducted for the two reflector nodes and one fuel node at each end of the core as depicted in Fig. 7 with vacuum boundary conditions used at the outer boundary of the reflector and the boundary conditions from the global calculation used at the outer boundary of the fuel node. The node-homogenized parameters and DFs determined for each of the three nodes from the extended assembly calculation are then used in the next iteration of the global calculation.

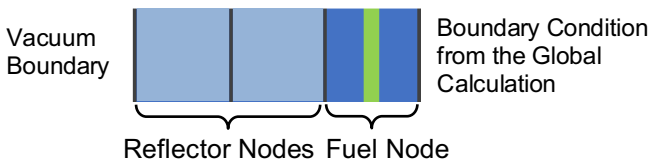


**Figure 7. Extended Assembly Calculation for the Reflector Nodes (Shown for Left End of the Core)**

## 5. RESULTS

Fig. 8 show the variation in the leakage-corrected DFs between the left and right boundaries of each node for the steady state case and for the transient state at 0.5 s as determined by the time-dependent homogenization technique. For comparison Fig. 8 also shows the ADFs from Table V for each node.

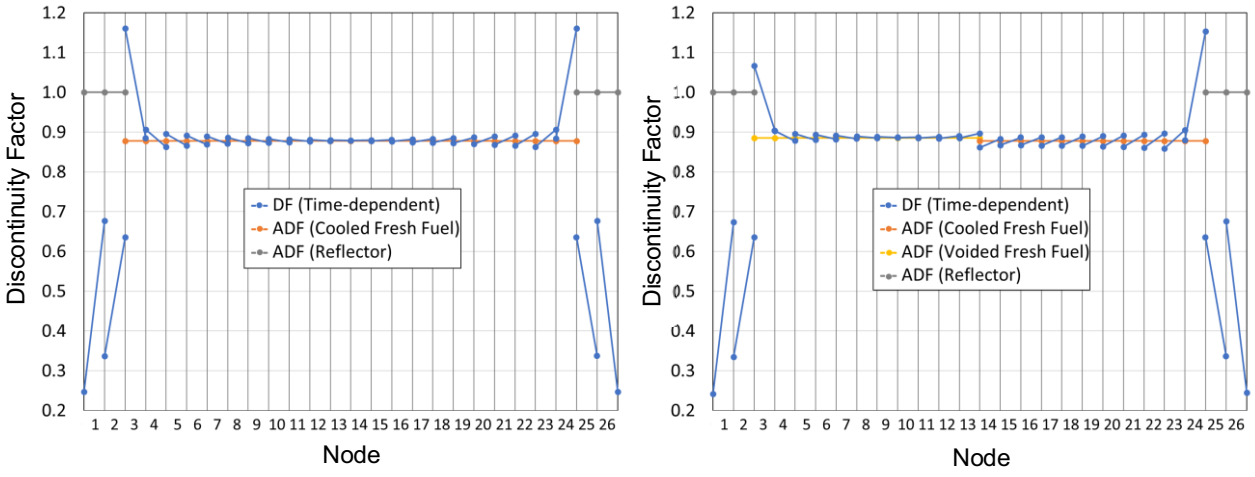


a) Steady State Configuration (Group 1) b) Transient State at 0.5 s (Group 1)

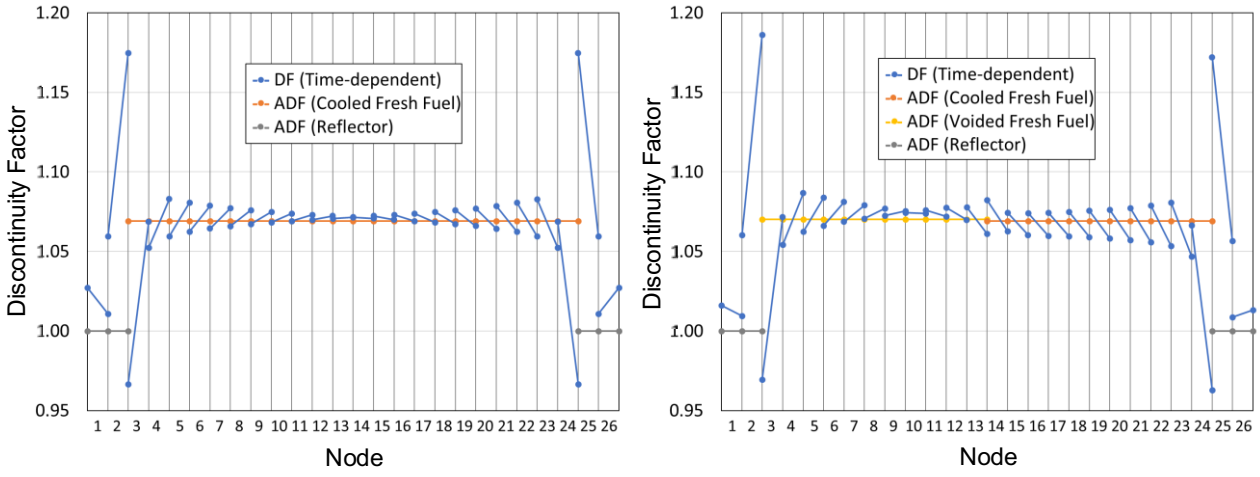


a) Steady State Configuration (Group 2) b) Transient State at 0.5 s (Group 2)

**Figure 8. Time-dependent Discontinuity Factors and Assembly Discontinuity Factors**

Fig. 8 shows how the magnitude of the difference in the DFs between the left and right boundaries of the nodes is influenced by the gradient of the fluxes across the nodes seen in Figs. 4 and 5. In the steady-state case, the flux gradient approaches zero for the nodes at the core midpoint (i.e. nodes 13 and 14) for which the DFs closely match the ADF value for cooled fuel. The largest difference in the DFs in seen in the reflector nodes, where the fluxes approach zero at the core boundaries, and in the fuel nodes at the core-reflector interface. In the transient case, the DFs of node 10 approach the value for the ADF for voided fuel since node 10 experiences the highest fluxes (see Fig. 5) and thus has a flux gradient that approaches zero.

Fig. 9 shows the variation, expressed as a percent difference, in the DFs of node 14 over the course of the transient with respect to the steady state values. From Fig. 8, the DFs at time 0 very closely match the ADF value for cooled fuel. During the transient node 14 remains cooled whereas node 13 is voided. Even though the material properties of node 14 do not change during the transient, the DFs change by as much as 2%. As the transient proceeds, the DFs approach constant values indicating that the shape of the flux around node 14 is no longer changing. However, the DFs for node 14 are no longer the same values that they were at steady state, unlike in the case of the ADFs.

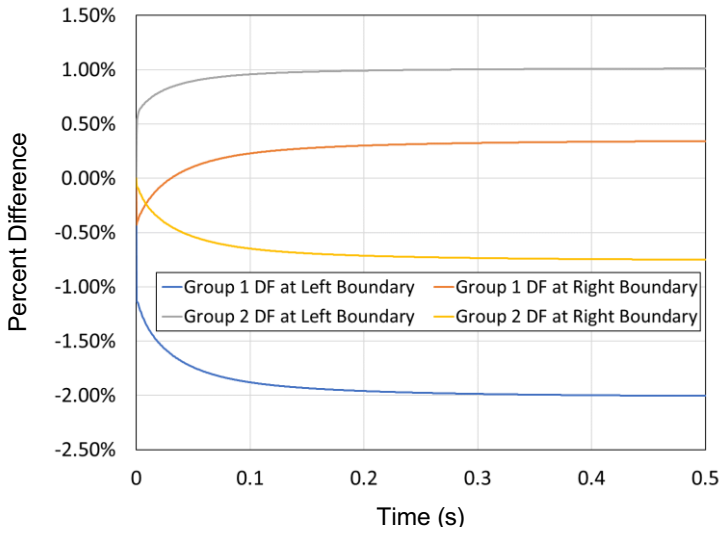


**Figure 9. Variation in Time of the Discontinuity Factors for Node 14 with Respect to the Steady State Values**

Figs. 10, 11 and 12 show the nodal variation in the percent difference over the course of the transient between the three homogenization techniques and the node-averaged reference solution for the fast flux, the slow flux and the fission-neutron production rates, respectively. The percent difference is calculated for each node via eqn. (1)

$$\Delta_i\% = \frac{x_j^h(t) - x_j^r(t)}{x_j^r(t)} \times 100\% \qquad (1)$$

where $x_j^h(t)$ is the quantity of interest at time $t$ for the $j^{\text{th}}$ node of the homogeneous solution and $x_j^r(t)$ is the node-averaged reference value to which $x_j^h(t)$ is compared.

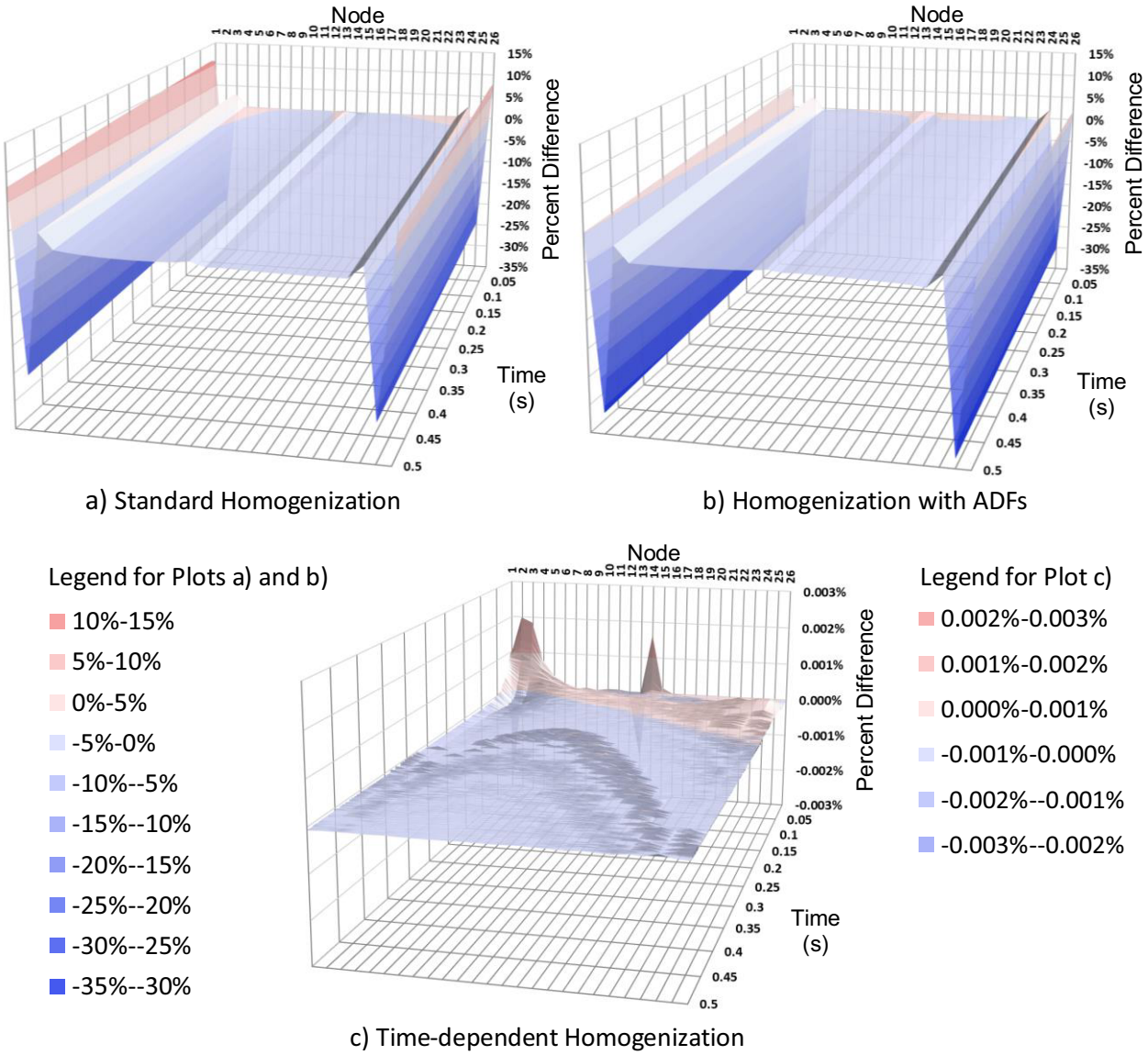


**Figure 10. Percent Differences between the three Homogenization Techniques and the Node-averaged Reference Solution for the Fast Flux**

In Fig. 10, the percent differences for the fast fluxes is relatively constant for fuel nodes 4 to 23 for the standard homogenization and the homogenization with ADFs, ranging from an average of 0.05% at time 0 to an average at time 0.05 s of -3.6% for the standard homogenization and -4.5% for the homogenization with ADFs. In contrast, the average percent difference for the time-dependent homogenization for the same fuel nodes is 0% at time 0 and -0.00006% at time 0.05 s. Larger discrepancies occur in the reflector nodes and in fuel nodes 3 and 24 adjacent to the reflector nodes. The maximum difference is -28% and -33% in node 25 for the standard homogenization and the homogenization with ADFs, respectively, occurring at transient time 0.5 s while the maximum difference for the time-dependent homogenization is only -0.02% occurring in node 1 during the first transient time step (i.e. at 0.0005 s).

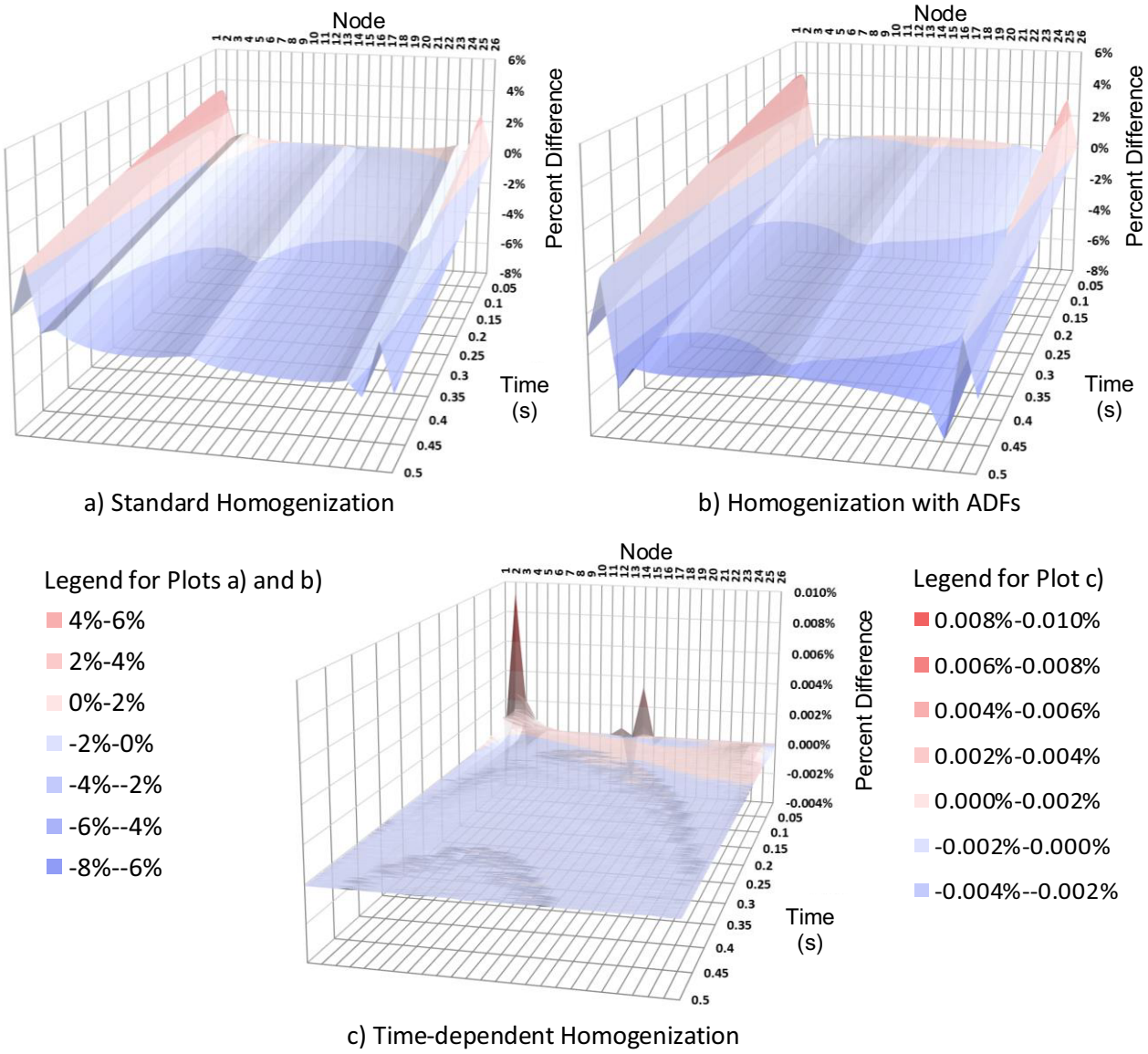


**Figure 11. Percent Differences between the three Homogenization Techniques and the Node-averaged Reference Solution for the Thermal Flux**

Similar to Fig. 10, the percent differences in Fig. 11 for the slow fluxes is relatively constant for fuel nodes 4 to 23 for the standard homogenization and the homogenization with ADFs, ranging from an average of 0.07% at time 0 to an average at time 0.05 s of -3.6% for the standard homogenization and -4.5% for the homogenization with ADFs. The average percent difference for the time-dependent homogenization for fuel nodes 4 to 23 is 0% at time 0 and -0.00005% at time 0.05 s. The discrepancies in the reflector nodes and in fuel nodes 3 and 24 are much smaller than those observed for the fast flux in Fig. 10. The maximum difference is only -4.5% and -6.5% in node 25 at time 0.5 s for the standard homogenization and the homogenization with ADFs, respectively, and only -0.01% in node 1 at time 0.0005 s for the time-dependent homogenization.

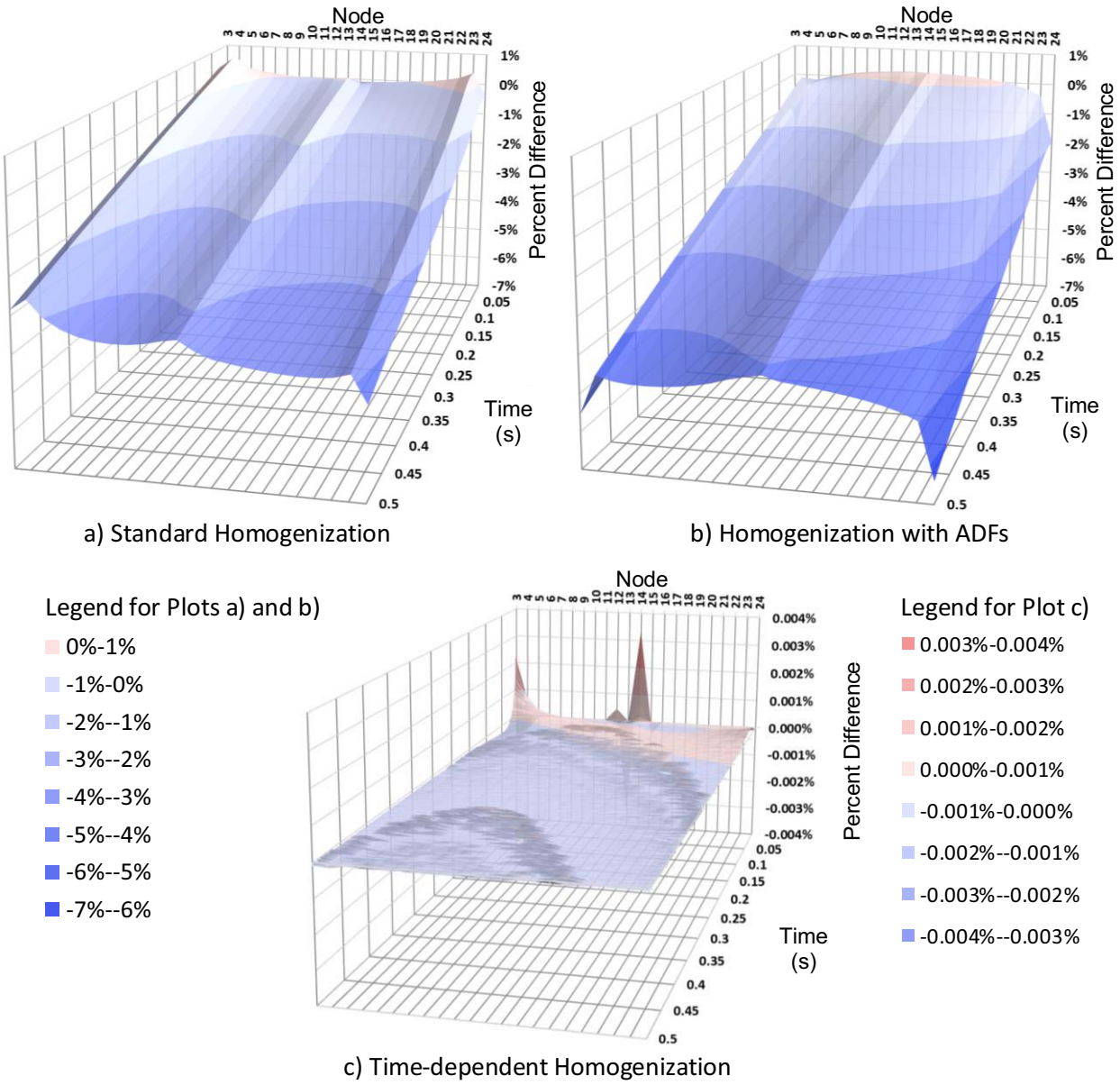


**Figure 12. Percent Differences between the three Homogenization Techniques and the Node-averaged Reference Solution for the Fission-Neutron Production Rates**

Similar to the fluxes in Figs. 10 and 11, the percent differences in Fig. 12 for the neutron production rates for fuel nodes 4 to 23 ranges from an average of 0.05% at time 0 to an average at time 0.05 s of -3.6% for the standard homogenization and -4.5% for the homogenization with ADFs. The average percent difference for the time-dependent homogenization for fuel nodes 4 to 23 is 0% at time 0 and -0.00006% at time 0.05 s. Larger discrepancies occur in fuel nodes 3 and 24 adjacent to the reflector nodes with the maximum difference being -4.5% and -6.4% in node 24 for the standard homogenization and the homogenization with ADFs, respectively. For the time-dependent homogenization the maximum difference is -0.004% which occurs in nodes 13 and 14 during the initial time step of the transient. At time 0.5 s, the total fission-neutron production rate for

the core is 38.2 n/s for the standard homogenization and 37.8 n/s for the homogenization with ADFs while for the time-dependent homogenization the total production rate matches the reference value of 39.2 n/s.

Fig. 13 shows the variation in time of the root mean square (RMS) percent difference of the fast flux, the slow flux, and the fission-neutron production rates. The RMS percent difference is calculated for the via eqn. (2)

$$RMS\% = \frac{1}{\frac{1}{N}\sum_{j=1}^{N} x_j^r(t)} \sqrt{\frac{1}{N}\sum_{j=1}^{N}\left(x_j^h(t) - x_j^r(t)\right)^2} \times 100\% \qquad (2)$$

where $x_j^h(t)$ and $x_j^r(t)$ are as defined for eqn. (1) and N is the total number of nodes.

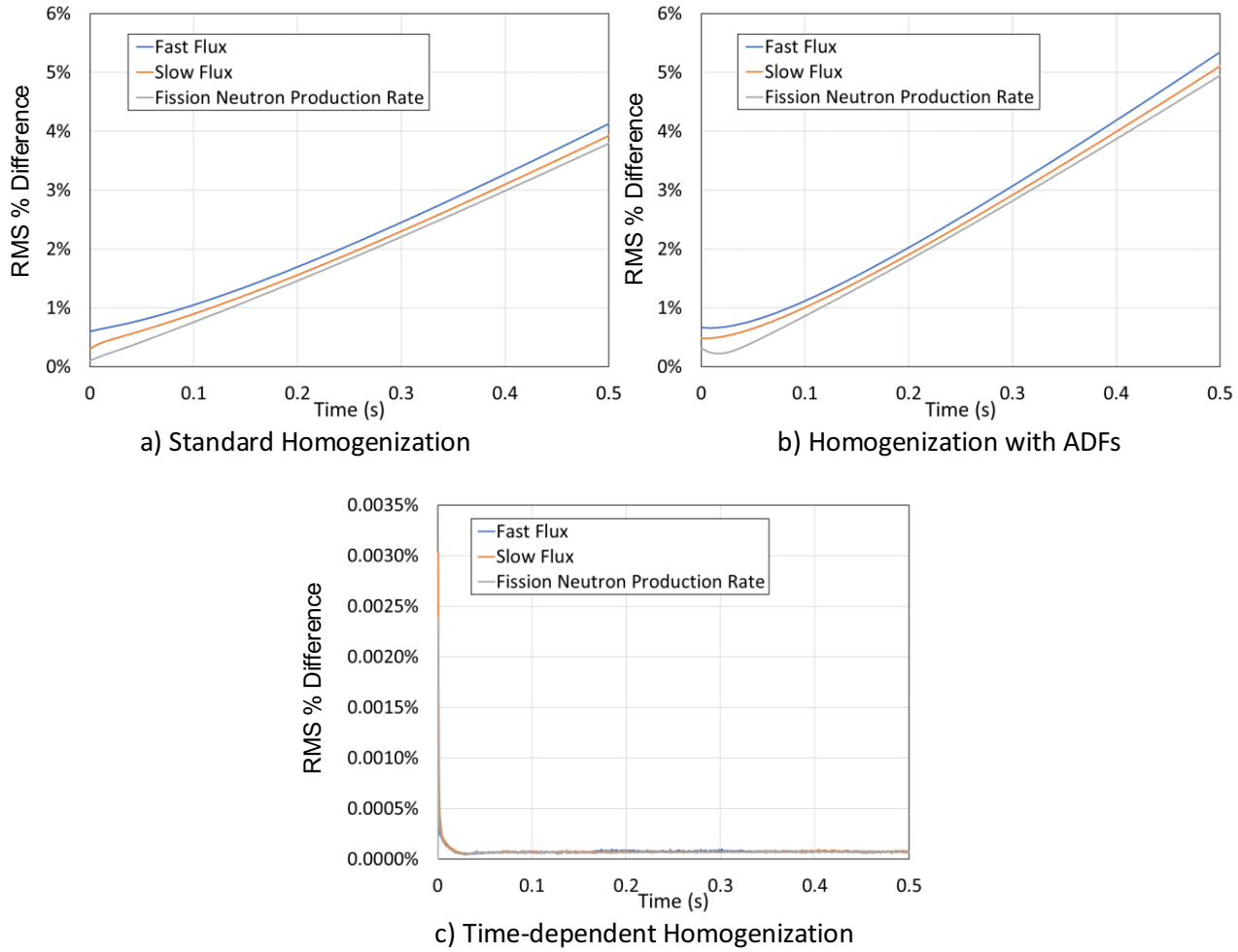


**Figure 13. RMS Percent Differences between the three Homogenization Techniques and the Node-averaged Reference Solution**

The RMS percent differences in Fig. 13 continually increases over the course of the transient for the standard homogenization and the homogenization with ADFs, reaching values of approximately 4% and 5%, respectively, at time 0.5 s while for the time-dependent homogenization, the differences remain constant at 0.00007% after reaching a maximum value 0.003% during the initial time step of the transient. Assuming the RMS percent differences increase linearly beyond 0.5 s for the standard homogenization and the homogenization with ADFs, then their differences would effectively double after 1.0 s whereas the differences would remain negligible for the time-dependent homogenization. Also, using ADFs, which are not leakage-corrected, results in a larger RMS difference for the standard homogenization technique.

Table VI compares the computational effort of each of the homogenization techniques investigated with respect to the reference solution.

**Table VI. Computational Effort with Respect to the Reference Solution**

| Homogenization Technique | Ratio of the Number of Finite Difference Calculations Performed with Respect to the Reference Solution |
|---|---|
| Standard Homogenization | 0.12 |
| Homogenization with ADFs | 0.12 |
| Time-dependent Homogenization | 0.58 |

The global-local iterative scheme used for the time-dependent homogenization results in a homogenization technique that, although more computationally intensive than the standard homogenization and the homogenization with ADFs, yields results that are essentially identical to the node-averaged values of the reference solution while requiring fewer calculations than the reference solution.

## 6. CONCLUSIONS

A recently developed GET-based time-dependent homogenization technique [1] that updates the nuclear parameters and the leakage-corrected DFs for every node at each time step is used to model the partial voiding of a 1D, 2G PHWR core. The core model consisting of 22 fuel nodes with two reflector nodes at either end to which vacuum boundary conditions are applied. The developed technique shows excellent agreement with the reference, heterogeneous-node, fine-mesh calculation with respect to the node-averaged fluxes and the node-integrated fission-neutron production rates. A maximum RMS percent difference of 0.03% occurs in the initial transient time-step which then quickly decreases and remains constant at a negligible 0.00007%. In contrast to time-dependent homogenization, standard homogenization uses a single set of nuclear parameters and ADFs for a given fuel type that are not updated in time. Using only the nuclear parameters from the standard homogenization with no ADFs, the modelling of the PHWR core voiding yield RMS percent differences that steadily increase during the transient, reaching approximately 4% after 0.5 s. When ADFs, which are not leakage-corrected, are included in the modelling, the RMS percent differences increase to approximately 5%. Finally, the time-dependent homogenization technique requires approximately one-third fewer finite-difference calculations than the reference calculation to achieve the same results.

## NOMENCLATURE

ADF – assembly discontinuity factor
BWR – boiling water reactor
DF – discontinuity factor
GET – generalized equivalency theory
PHWR – pressurized heavy water reactor

## REFERENCES

1. P. Schwanke and E. Nichita, "GET-based Time-Dependent Lattice Homogenization Using a Global-Local Approach", *Annals of Nuclear Energy*, **134**, pp. 359-369 (2019).
2. K. S. Smith, "Assembly Homogenization Techniques for Light Water Reactor Analysis", *Progress in Nuclear Energy*, **17**(3), pp. 303-335 (1986).
3. G. Marleau, A. Hébert, and R. Roy, *A User Guide for DRAGON Release 3.06L*, École Polytechnique de Montréal, Montréal, Québec, Canada (2013).
4. A. Koning, R. Forrest, M. Kellett, R. Mills, H. Henriksson, and Y. Rugama (Eds.), *The JEFF-3.1 Nuclear Data Library*, JEFF Report 21, OECD/NEA, Paris, France (2006).
5. K. Ott and R. J. Neuhold, *Introductory Nuclear Reactor Dynamics*, pp. 15, American Nuclear Society, La Grange Park, Illinois, USA (1985).
6. J. R. Lamarsh and A. J. Baratta, *Introduction to Nuclear Engineering, 3rd Ed.*, pp. 82, Prentice Hall, Upper Saddle River, New Jersey, USA (2001).
7. Benchmark Problem Committee of the Mathematics and Computation Division of the American Nuclear Society, "Argonne Code Center: Benchmark Problem Book", pp. 130, ANL-7416, Supplement 1, Argonne National Laboratory, Argonne, Illinois, USA (1972).
8. C. L. Hoxie, "Application of Nodal Equivalence Theory to the Neutronic Analysis of PHWRs" (PhD Thesis), Department of Nuclear Engineering, M.I.T, Cambridge, Massachusetts, USA (1982).